2023

Experimental Investigation of Heat Transfer to a Dual Jet Flow with Varying Velocity Ratio

Paula J. Murphy
Trinity College Dublin, Ireland

Sajad Alimohammadi
Technological University Dublin, sajad.alimohammadi@tudublin.ie

Seamus M. O'Shaughnessy
Trinity College Dublin, Ireland

2023 22nd IEEE Intersociety Conference on Thermal and Thermomechanical Phenomena in Electronic Systems (ITherm) | 979-8-3503-2166-1/23/$31.00 ©2023 IEEE | DOI: 10.1109/ITHERM55368.2023.10177606

Experimental investigation of heat transfer to a dual jet flow with varying velocity ratio

Paula J. Murphy[1,2], Sajad Alimohammadi[3], Séamus M. O'Shaughnessy[1]
[1]*Dept. of Mechanical, Manufacturing and Biomedical Engineering, Trinity College Dublin, Dublin, Ireland*
[3]*School of Mechanical & Design Engineering, Technological University Dublin, Dublin, Ireland*
[2]Email: murphp32@tcd.ie, ORCID ID: 0000-0002-1981-223

***Abstract*—Dual jet flow is a topical area of research due to their wide range of current and potential uses in industry. Despite this, there is still a lack of published studies which focus on the characterization of dual jet flow, particularly regarding their heat transfer capabilities. The objective of this investigation is to therefore build upon the available dual jet data and conduct an experimental study which focusses on the effect of the jet velocity ratio on heat transfer to a dual jet flow for a constant offset ratio of 3, where air is used as the working fluid. The wall and offset jet velocities are each varied between $5500 \leq Re \leq 12000$ to create a range of velocity ratios from $0.5 \leq V_r \leq 2$. A uniform heat flux of 2500 W/m² is maintained in the bounding wall and the local Nusselt number data is derived from temperature measurements acquired through infra-red thermography. The results show a strong dependence on the velocity ratio, where, for a constant total mass flow rate, increasing the velocity ratio increased the value of a localized minimum Nusselt number and moved its location closer to the jet exit. In addition, increasing the total mass flow rate elevated Nu_x across all downstream locations for each V_r examined.**

Keywords—dual jet, single offset jet, single wall jet, convective cooling, heat transfer, velocity ratio

I. INTRODUCTION

The term 'wall jet' refers to a stream of fluid discharged tangentially along a solid boundary. If this stream of fluid is offset from the boundary by some distance, it becomes an offset jet. In the context of this research, the combination of a wall jet and offset jet is referred to as a dual jet. Dual jet flow behaviour is highly complex and distinctly different to that of wall and offset jets. This flow arrangement has a wide range of uses in industry, including fuel injection arrangements, noise suppression techniques, and wastewater evacuation. Due to the enhanced mixing associated with dual jet flows and straightforward scalability, they are commonly used across many heat transfer applications, such as gas turbine blade shielding, electronics cooling, de-icing of aircraft wings, and air conditioning systems [1-3]. In these instances, the wall jet and offset jet velocities may differ greatly, which may be deliberate (*e.g.,* using a low-velocity wall jet to stabilize a much larger offset jet while cooling during a blow molding process), or incidental (*e.g.,* wastewater evacuation to rivers or streams) [4]. While dual jet flow remains severely underrepresented in the published literature, the effect of the ratio between the wall and offset jet velocities is studied to an even lesser extent, and yet to be examined through experimental means.

Irish Research Council (GOIPG/2019/3719).

The typical planar dual jet flow structure is shown in Fig. 1 for a wall jet and offset jet of equal width w. The jets are ejected with velocities U_w and U_o respectively, where the velocity ratio is defined as $V_r = U_w/U_o$ [5, 6]. The non-dimensionalised separation distance between the two jet exits is termed the offset ratio, *i.e.,* $OR = d/w$, and the Reynolds number for each jet is determined with respect to w as per equation (1), where ν is the fluid kinematic viscosity.

$$Re = \frac{U_{jet} w}{\nu} \tag{1}$$

The dual jet flow structure can be divided into three distinct downstream regions, *i.e.,* the converging region, the merging region, and the combined region. The converging region is defined by the existence of the recirculation zone, a low-pressure region located directly downstream of the jet exit induced by the mutual entrainment between the wall jet and the offset jet [7]. This causes the offset jet to deflect towards the wall jet. They eventually converge at the merge point (mp), at which point the mean streamwise velocity u is 0 m/s [5]. The merging region hence encapsulates the interaction between the two jets, before becoming fully combined at the combined point (cp), identified as the furthest downstream distance at which $du/dy = 0$. Beyond this point in the combined region, the dual jet behaves in a similar manner to a single equivalent wall jet [5].

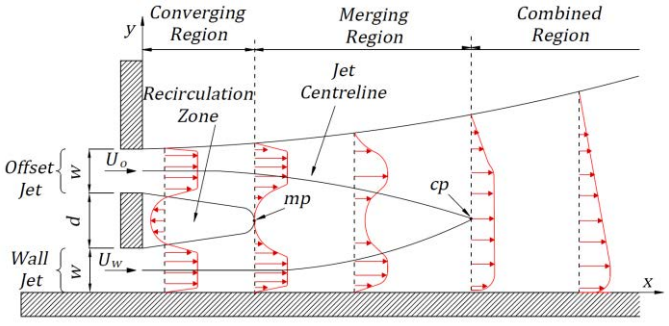

Fig. 1. Dual jet flow structure

The first, and to our knowledge, only published experimental study relating to dual jet flow was conducted by Wang and Tan [5], who investigated the flow field for $Re = 10{,}000$, $OR = 1$ and $V_r = 1$ using particle image velocimetry (PIV) techniques.

In doing so, an unsteady flow regime was observed, where vortical structures were shed downstream of the recirculation zone in a periodic von Karman-like fashion, which was later simulated by Li *et al.* [8] using Large Eddy Simulation (LES). Dual jet flow behaviour was further examined by Kumar and Das [3] through numerical means, whose findings highly contrasted that of Wang and Tan [5]. In this instance, a steady flow phenomenon was noted, where two counter-rotating vortices were observed within the recirculation region. The onset of such instabilities in dual jet flow was later investigated by Mondal *et al.* [9], who detected von Karman-like vortex shedding for an offset ratio range between $0.7 \leq OR < 2.1$, and two counter-rotating vortices were observed for all other OR for $Re = 10{,}000$.

While the flow behaviour associated with dual jets is described in the literature to some degree, studies which focus on their corresponding heat transfer characteristics exist to a much lesser extent. Vishnuvardhanarao and Das [6] conducted the first numerical heat transfer study, analyzing the effect of the effect of the Reynolds number and velocity ratio on the downstream local Nusselt number profile (Nu_x). In doing so, a clear rise in Nu_x was evident for increasing Re, and Nu_x was greatest at all locations when U_w dominated. The influence of the offset ratio was hence investigated by both Farooq and Das [10] and Kumar [11], where the Nu_x profiles presented by Farooq and Das [10] appeared quite oscillatory in nature, while those of Kumar [11] were characterized by two distinct peaks for all $OR > 2$. Mondal *et al.* [12] subsequently studied the effect of varying both Re and the Prandtl number, along with the thickness and conductivity of the bounding wall. Hnaien *et al.* [13] investigated the impact of the wall inclination angle, before further exploring the effect of changing Re and OR in Hnaien *et al.* [14]. Rathore *et al.* [15] introduced different inlet temperatures for the wall and offset jets, and Assoudi *et al.* [16] further examined this jet inlet temperature ratio. The potential enhancement in the heat transfer that can be acquired through the use of a wavy bounding wall was first investigated by Singh *et al.* [17] and continued through several follow up studies. In recent studies, Hnaien *et al.* [18] and Mondal *et al.* [19] combined a dual jet arrangement with a parallel co-flow, where an increase in the co-flow velocity was found to decrease the average surface Nusselt number $\overline{Nu_x}$. Finally, Mondal and O'Shaughnessy [7] investigated the effect of replacing the wall jet with a second offset jet, termed a dual offset jet, where the addition of a second recirculation region induced noticeably different cooling characteristics.

However, all published studies relating to the heat transfer characteristics of dual jet flow carried out to date have been entirely numerical in nature. A summary of the turbulence models implemented in each case can be found in Table I. The experimental study conducted by Wang and Tan [5] focused on flow behaviour only, for a single Re and OR value, and thus does not provide the necessary empirical Nu_x data needed to validate the findings from all subsequent numerical studies. In the vast majority of cases, the numerical models were validated based on the published experimental studies relating to single offset jets, such as Vishnuvardhanarao and Das [6] and Mondal *et al.* [12]. However, as single offset jets flow behaviour is distinctly different, it may not be a sufficient means of validation. A jet arrangement similar to that of a dual jet is featured in an experimental investigation carried out by Gao *et al.* [4], however the scope of this study does not quite align with a dual jet characterization, as the focus in this case was to stabilize a much larger offset jet through the use of a thin co-flowing wall jet. As the range of parameters are quite limited, the experimental data provided cannot be used to validate a numerical dual jet study. [8]

TABLE I. SUMMARY OF TURBULENCE MODELS USED IN PUBLISHED NUMERICAL DUAL JET STUDIES

Authors	Turbulence Model
Li et al. [8]	LES
Vishnuvardhanarao and Das [6]	k − ε
Farooq and Das [10]	k − ε
Kumar [10]	k − ε
Kumar and Das [3]	k − ε
Mondal *et al.* [9]	k − ε
Mondal *et al.* [12]	k − ε
Hnaien *et al.* [13]	k − ω
Assoudi *et al.* [16]	RSM
Rathore *et al.* [15]	Laminar
Singh *et al.* [17]	k − ε
Mondal *et al.* [19]	k − ω
Mondal and O'Shaughnessy [7]	k − ε

The primary aim of the current investigation is to build upon the available experimental data relating to dual jet flows and to generate new heat transfer data from which important insights can be inferred regarding their control and optimization. An initial experimental study conducted by the authors [20] analysed the effect of the Reynolds number on the surface Nusselt number profile for $OR = 3$ and $V_r = 1$. In doing so, a distinct Nu_x trend was observed, where Nu_x initially decreased with increasing downstream distance until reaching a location which, most likely, coincides with the merge point. Beyond this, Nu_x increased towards a local maximum as the jets interacted and subsequently decreased with further downstream distance. This trend was found to remain unchanged with varied Re values, where the location of the local minimum and local maximum were consistent, but an increase in the Reynolds number led to a corresponding increase in Nu_x at all downstream locations. Further to this, $\overline{Nu_x}$ was found to increase linearly with increasing Re. The present research aims to expand upon these findings, where, using air as the working fluid, the effect of changing the velocity ratio for a given volumetric flow rate is investigated for $OR = 3$. A uniform heat flux (UWF) is maintained in the bounding wall and changes in Nu_x and $\overline{Nu_x}$ are analysed.

II. METHODOLOGY

A. Experimental Setup

The experimental rig used for this investigation is shown in Fig. 2. The wall jet and offset jet have identical slot jet nozzle exits of width $w = 7\ mm$. A jet aspect ratio $AR = 30$ ensures consistent 2-D behaviour along the mid-plane of the flow domain, as per Wang and Tan [5]. The addition of smooth side and top walls, *i.e.*, the enclosure, also aid in this regard, as

discussed by Nasr and Lai [21], and reduce the influence of external environmental factors. This allows for a planar analysis of the experimental results along the midplane of the flow domain, *i.e.*, $Z = z\ /\ w = 0$. The height of the enclosure, equal to $35.1w$, was chosen based on the water level height of $30w$ used in Wang and Tan [5].

The air supply to each jet is provided from two separate AXAIR GREG9 160x62R 230/1/50/60 centrifugal single inlet blowers. The flowrate can be adjusted independently for each jet. The blowers are mounted on a standalone structure and connected via flexible hosing to mitigate the transmission of vibrations downstream. The turbulence present in the airflow is reduced to an acceptable level inside the airflow conditioning chamber, where the additional 1 m length of rigid PVC piping protects the incoming airflow to the chamber from upstream conditions. The airflow conditioning chamber is comprised of three sections, namely the settling chamber, the contraction and the nozzle, where the design for each section is based primarily on the work of Mehta and Bradshaw [22]. The flow straightening components are located within the settling chamber where the flow velocity is lowest and include a series of screen meshes and a honeycomb flow straightener. These devices act to reduce the lateral and longitudinal variations in the flow, respectively, and help create a uniform cross sectional flow velocity. The contraction increases the flow velocity in advance of the nozzle exit and further reduces lateral flow variations, where the contraction length and shape were determined using the procedure outlined by Morel [23]. The flow rate through the chamber is monitored based on the measured pressure drop across the honeycomb flow straightener using a Sensirion SDP1000 differential pressure sensor, where a linear relationship was previously established between the volumetric flowrate and the pressure drop.

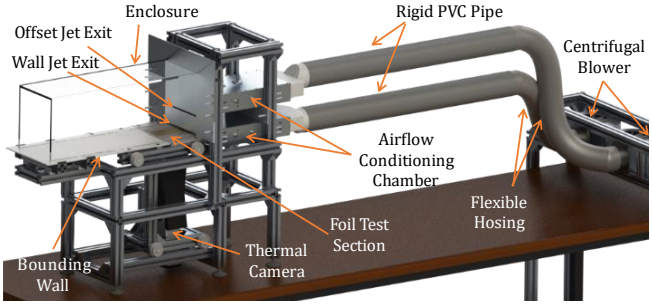

Fig. 2. Experimental setup

An approximate uniform wall flux UWF condition is attained in the bounding wall along the region of interest using an ohmically heated 25 μm thick Inconel 625® foil, where the region of interest extends from the nozzle exit to approximately 18.5 jet widths downstream. A tensioning mechanism is used to prevent the foil warping at higher temperatures and the underside of the foil is painted with a thin matte black layer to ensure an emissivity of 0.95 for the purpose of acquiring thermal measurements. An YF3 ZnS anti-reflection coated germanium window is used to establish a 10 mm air gap beneath the foil and constrain heat losses to the upper surface. Conduction through the air gap is monitored through the use of a T-type thermocouple. Two additional T-type thermocouples respectively determine the wall jet and offset jet temperatures inside their corresponding airflow conditioning chambers. Beyond the heated foil region of interest, the bounding wall consists of a smooth Perspex sheet which brings the total length of the downstream domain to 700 mm.

The temperature distribution on the underside of the foil is measured using a FLIR A655sc IR camera at a capture rate of 25 Hz. The temperature difference between the top and bottom surface of the foil is considered negligible due to the sufficiently small foil thickness. The IR camera can view a foil test area of 18.5 jet widths downstream (x-direction) and $\pm$3.5 jet widths across the jet centerline (z-direction), where the jet centerline is aligned along $z = 0$ and $x = 0$ corresponds to the nozzle exit. For the purpose of analysis, all measurements in the x- and z-directions are non-dimensionalised with respect to the jet width, such that $X = x/w$ and $Z = z/w$.

Throughout testing, a heat flux of approximately 2500 W/m^2 maintained in the bounding wall, monitored by measuring the voltage drop across the foil V for a constant current supply I. This heat flux value was chosen as it induces adequately measurable temperature gradients within the foil while minimizing heat losses to the surrounding ambient and maintaining the foil surface temperature below a safe level, suitable for the laboratory environment. A tailored LabVIEW program collects and records all measured values and controls the airflow to each jet using a National Instruments data acquisition system. The experimental setup can achieve a jet Reynolds number from 5500 to 12000 per jet, which can be adjusted individually to provide the experimental jet velocity ratio range of $0.5 \leq V_r \leq 2$. For this study, the offset ratio is maintained at a constant value of $OR = 3$ and each jet Reynolds number is adjusted to examine a) the effect of increasing the total mass flow rate for a given velocity ratio and b) the effect of adjusting the velocity ratio for a constant total mass flow rate, where the total mass flow rate is constant for a specified total Reynolds number Re_{tot}, *i.e.*, $Re_{tot} = Re_w + Re_o$. For each dual jet configuration, data is collected over a 20 second time interval, where it is ensured that the system receives the necessary recovery time between tests to reach a steady state, indicated through monitoring various flow and thermal parameters.

B. Data Reduction

The thermal imaging measurement system allows for the local Nusselt number on the foil surface to be established on a per-pixel basis, where each pixel has dimensions $dx\ (mm) \times dz\ (mm)$. Hence, using the surface temperature measurement T_s provided, Equation (2) can used to establish Nu_x at each pixel location, where h is the local heat transfer coefficient, k_{air} is the air thermal conductivity and the jet temperature T_{jet} is an average of the wall jet and offset jet temperatures.

$$Nu = \frac{hw}{k_{air}} = \left(\frac{q''_{conv}}{T_s - T_{jet}}\right) \times \frac{w}{k_{air}} \qquad (2)$$

In equation (2), the term q''_{conv} refers to the convective heat flux induced by the dual jet flow and is determined through a heat energy balance on the foil surface for each pixel. This is achieved using the method outlined in Gibbons *et al.* [24], *i.e.*, equation (3), where q''_{conv} is equated to the ohmic heat

generation within the foil (q''_{gen}) minus various identified sources of heat loss. These sources include conduction through the insulating air gap (q''_{cond}), radiation to the germanium window (q''_{rad}), lateral conduction within the foil (q''_{lc}) and the capacitive heating of the foil (q''_{cap}).

$$q''_{conv} = q''_{gen} - q''_{cond} - q''_{rad} - q''_{lc} - q''_{cap} \quad (3)$$

The ohmic heat generation within the foil is calculated using equation (4), where A_f is the total foil area.

$$q''_{gen} = \frac{IV}{A_f} \quad (4)$$

Fourier's law is employed to determine the heat loss via conduction through the insulating air gap, *i.e.*, equation (5), where T_{ag} is the measured temperature inside the air gap and d_{ag} is the perpendicular distance from the underside of the foil to the point of measurement.

$$q''_{cond} = -k_{air}\frac{(T_{ag} - T_s)}{d_{ag}} \quad (5)$$

The radiative heat transfer between the foil and the germanium window is calculated based on the infinite parallel plate assumption, as per equation (6). In this equation, ε_p and ε_{Ge} denote the emissivities of the matte black paint layer and the germanium window, respectively, T_{Ge} is the temperature of the germanium window and σ is the Stefan Boltzmann constant.

$$q''_{rad} = \frac{\sigma(T_s^4 - T_{Ge}^4)}{\frac{1}{\varepsilon_p} + \frac{1}{\varepsilon_{Ge}} - 1} \quad (6)$$

The lateral conduction within the foil is determined using equation (7), where the minus sign indicates the direction of heat transfer. In this expression, the subscripts f and p refer to the foil and paint layers, respectively. The term k hence refers to the conductivity of the relevant material and δ is the associated layer thickness.

$$q''_{lc} = -\left(k_f\delta_f^2 + k_p\delta_p^2\right)\left(\frac{\partial^2 T_s}{\partial x^2} + \frac{\partial^2 T_s}{\partial z^2}\right) \times 2(dx + dz) \quad (7)$$

The final heat loss quantity, *i.e.*, the capacitive heating of the foil and paint layer, is calculated using equation (8), where ρ is the density of the substrate, C is the corresponding specific heat capacity value and $\frac{\partial T_s}{\partial t}$ represents the change in surface temperature with respect to time. However, as the experimental setup in the present investigation is allowed to reach a steady state between successive test cases, the surface temperature T_s does not change with time and, hence, the capacitive heating term reduces to approximately 0 W/m^2

$$q''_{cap} = \left(\rho_f C_f \delta_f + \rho_p C_p \delta_p\right)\frac{\partial T_s}{\partial t} \quad (8)$$

III. Results

A. Experimental Rig Validation

To validate the planar flow assumption for the experimental setup, the distribution of both T_s and Nu_x within the test foil are analysed, where the maximum experimental uncertainty of each was estimated at ±5.63% and ±11.4%, respectively, for a 95% confidence interval. A sample set of contour plots relating to $V_r = 0.5$ is shown in Fig. 3, where the time-averaged surface temperature and local Nusselt number are represented in Fig. 3(a) and Fig. 3(b) respectively. In each case, clear bands of constant value parallel to the nozzle exit are evident at all downstream locations, indicating near-identical flow and heat transfer behaviour at all Z locations. This suggests that the experimental setup successfully provided uniform planar flow inside the flow domain, which allows for the 2-D analysis of the output data. In addition, all surface variables are averaged with respect to the Z dimension for the remaining analysis to reduce random noise present in the datasets.

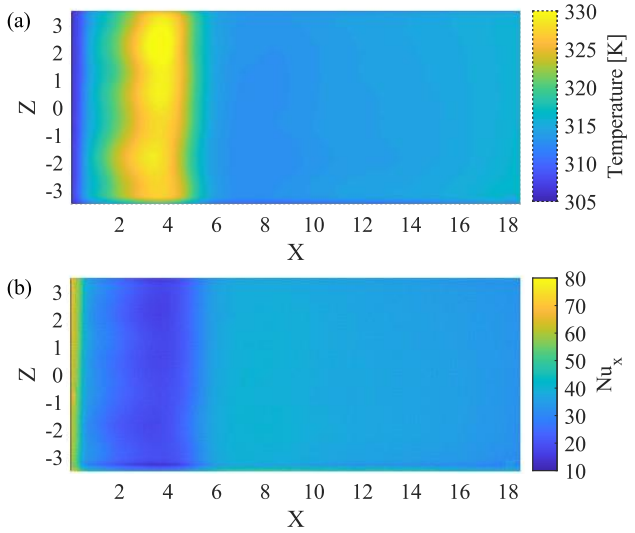

Fig. 3. Contour plot of time-averaged a) surface temperature and b) local Nusselt number for $V_r = 0.5$ case ($Re_w = 5500, Re_o = 11000$)

To further validate the credibility of output data from the experimental setup, the results produced for a single wall jet and a single offset jet are each compared to relevant published experimental data. This is shown in Fig. 4, where the time averaged local Nusselt number profile is displayed for both the single wall jet and single offset at $Re = 5500$, where the maximum Re uncertainty was estimated at ±5.36%.

The heat transfer findings associated with the single wall jet are generally as expected, as shown in Fig. 4, where an initial decrease in Nu_x at the nozzle exit coincides with the growth of the boundary layer and degradation of the potential core, followed by a rise in Nu_x as the boundary layer flow transitions to turbulent. The value of Nu_x eventually decreases with further downstream distance as entrainment with the quiescent surroundings reduces the mean jet velocity. This trend is reflected in the results published by AbdulNour *et al.* [25], however slight differences can be observed in the downstream scale due to the use of a contoured nozzle in the present investigation compared to the knife-edged nozzle used in the case of AbdulNour *et al.* [25].

Similarly, the single offset jet produces a downstream Nu_x trend consistent with previous published findings, such as that of Kim *et al.* [26] for a similar offset ratio, as shown in Fig. 4. As the jet exits from the nozzle exit, the initial decrease in Nu_x followed by a sharp increase is a consequence of the complex flow behaviour inside the recirculation region, where the local

maximum coincides with the downstream location of the reattachment point. The decline in Nu_x beyond this point occurs as the flow transitions to that of an equivalent wall jet, along with continuous entrainment from the surroundings. The features present in the Nu_x profile align closely with that of Kim *et al.* [26] regarding their downstream location, where the enhanced Nu_x magnitude in the case of Kim *et al.* [26] is due to the use of the much larger Reynolds number of 39,000.

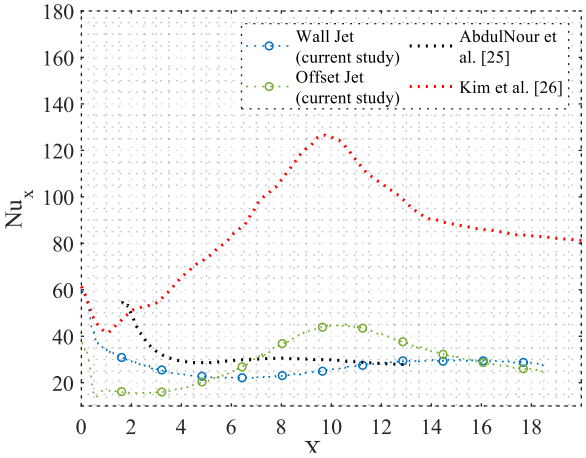

Fig. 4. Comparison of single wall jet and single offset jet data for $Re = 5500$ with the published experimental findings of AbdulNour et al. [25] (single wall jet) and Kim et al. [26] (single offset jet)

The repeatability of the output from the experimental setup is demonstrated in Fig. 5, where the Nu_x profile for a selection of Re is plotted alongside the output from their corresponding test repetition, where $V_r = 1$ in each case. A close alignment between the first and second test iteration can be observed for all Re, indicating that the experimental setup produces precise, repeatable results.

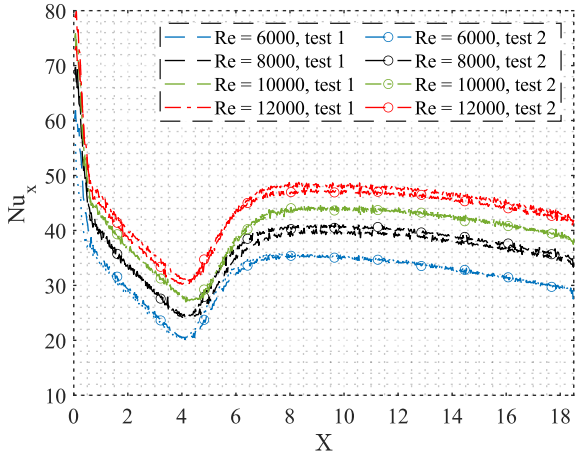

Fig. 5. Repeatability of Nu_x data for various Re

B. *Effect of Mass Flow Rate*

The plots presented in Fig. 6 demonstrate the effect of changing the total mass flow rate of the two jets, or R_{tot}, for a constant velocity ratio. Four velocity ratios were chosen in this case, where the number of plots available for each V_r was subject to the flow limitations of the experimental rig. Similar to the authors' prior study [20] for $V_r = 1$, a distinct Nu_x trend is evident throughout. In each case, Nu_x appears to decline with increasing downstream distance in the region spanning from the nozzle exit to the assumed location of the merge point, at which location a local minimum in the Nu_x profile exists. This behaviour corresponds to the growth of the boundary layer in this region, along with localized zero average flow velocity which defines the merge point. Beyond this point, the clear rise in Nu_x towards a local maximum value corresponds to the interaction between the two jets, where the increased mixing leads to enhanced heat transfer in the region. In the region past this local maximum, Nu_x generally declines with further downstream distance as the effect of entrainment with the quiescent surroundings starts to dominate and causes the mean jet velocity to decrease.

Overall, this trend remains relatively unchanged for each V_r value examined. The data in Fig. 6 also suggests that an increase in the total mass flow rate of the two jets leads to an enhancement in the heat transfer at all downstream locations, indicated by higher Nu_x values. The shape of the Nu_x profile is generally unaltered in each case, where an increase in the total mass flowrate simply shifts the curve upwards along the Nu_x axis by some relative amount for the V_r in question, and the X location of most downstream features is somewhat consistent. This is similar to the findings of the authors' preceding study [20], who, for $V_r = 1$, noted that an increase in Re increased the value of $\overline{Nu_x}$ in a linear manner and the downstream location of all notable characteristics in the Nu_x profile remained constant.

In this investigation however, slight differences can be observed. For all V_r shown in Fig. 6, the location of the local minimum seems to move upstream towards the nozzle exit with an increase in Re_{tot}, where Fig. 6(b) suggests a linear change for $V_r = 0.8$. In this instance, the location of the local minimum, and hence the merge point, appears to shift from $X = 5$ to $X = 4.5$ when R_{tot} is increased from 12500 to 20000, implying that a higher mass flow rate induces the jet interaction further upstream. Conversely, the position of the local Nu_x maximum remains approximately constant with respect to mass flow rate, meaning the downstream distance between the Nu_x minimum and maximum increases with increasing mass flow rate. It is also interesting to note that for $V_r = 1$, the data suggested that the merge point is likely to exist at $X = 4$ according to the author's prior study [20] for all Re investigated. However, as shown in Fig. 6(b), the assumed merge point associated with $V_r = 0.8$ occurs further downstream but appears to approach that of $V_r = 1$ with increasing mass flow rate.

All other V_r cases display a similar trend, however, as the lowest R_{tot} value considered in these instances is greater than that of the $V_r = 0.8$ case. The location of the Nu_x minimum for the lowest R_{tot} value exists closer to that of $V_r = 1$ and further increasing R_{tot} moves it upstream of this point. An anomaly does exist however in Fig. 6(a), relating to $V_r = 0.5$, where the merge point appears to move downstream for the largest R_{tot} value, *i.e.*, $Re_w = 6000$ and $Re_o = 12000$. In addition to this, the Nu_x profile appears to 'peak' in the location of the local maximum, which is at the same downstream location as the other Re_{tot} values examined, and a secondary maximum exists further downstream. This unique Nu_x profile is currently the

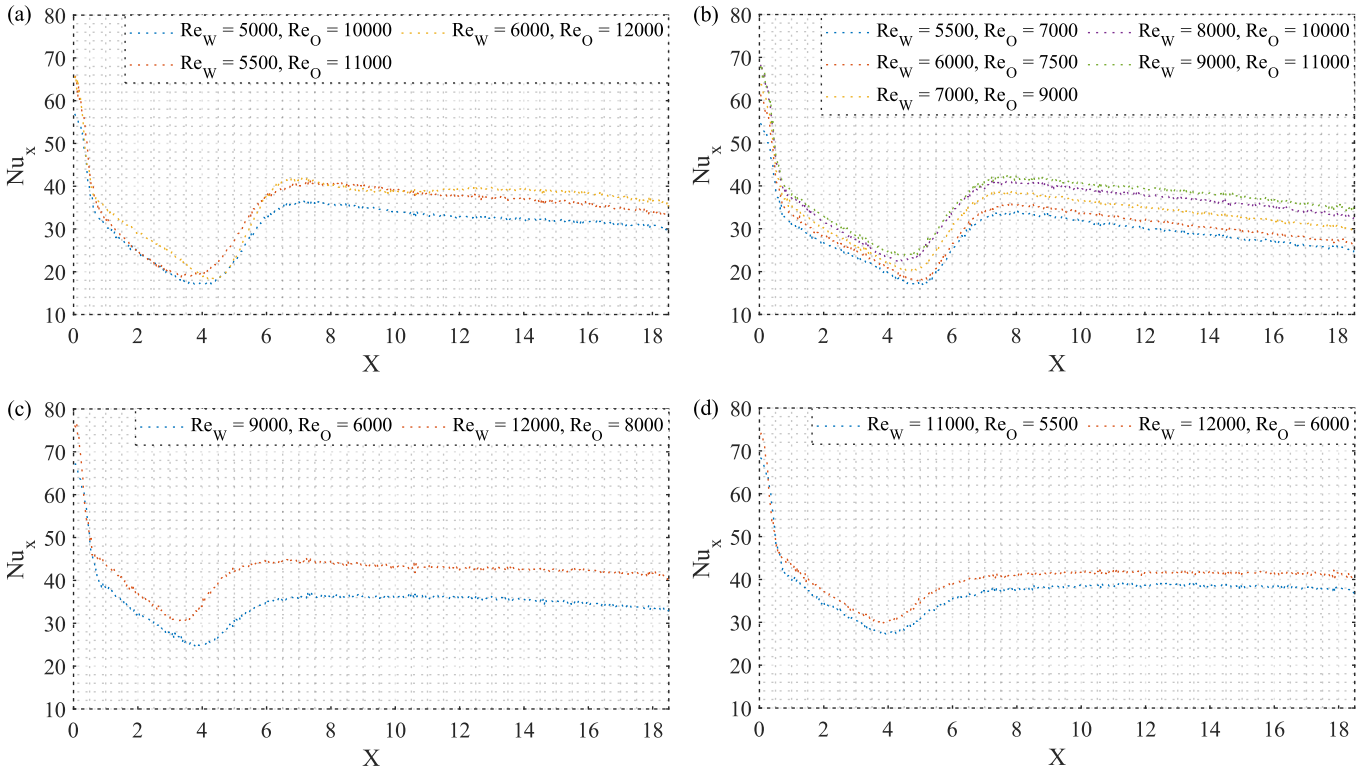

Fig. 6. Effect of changing total mass flow rate $\dot{m}$, and hence the total Reynolds number Re_{tot}, for a constant velocity ratio, where a) $V_r = 0.5$, b) $V_r = 0.8$, c) $V_r = 1.5$ and d) $V_r = 2$

subject of an ongoing computational fluid dynamics (CFD) and experimental particle image velocimetry (PIV) study to understand the different flow phenomena driving this heat transfer behaviour for this case. A final point to note relates to Fig. 6(c) and Fig. 6(d), which represent $V_r = 1.5$ and $V_r = 2$, respectively. For these two cases, the prominence of the local maximum seems to be much less compared to the previous cases, and the curve appears to flatten somewhat with downstream distance beyond this point. With the velocity ratio being greater than 1 in both cases, this heat transfer behaviour is most likely a feature of a wall jet dominating flow.

C. *Effect of Velocity Ratio*

The data presented in Fig. 7 shows the effect of changing V_r on the downstream Nu_x profile for a constant Re_{tot} value, where $Re_{tot} = 14000, 16000, 18000, 20000$. In general, the plots appear more closely grouped in the far downstream region, which is to be expected as the flow transitions to that of a single equivalent wall jet. However, the Nu_x plots associated with lower V_r values tend to continue to decline steadily over this region, whereas higher V_r values appear to level off or flatten. This would suggest that in the case of an offset jet dominating flow, the mean jet velocity must reduce at a much faster rate due to the jet interactions that are taking place. On the contrary, the mean jet velocity is preserved over a longer downstream distance in the case of a wall jet dominating flow.

Close to the nozzle exit, the dispersal of the various plots appears to depend on the value of Re_{tot}. For lower values of Re_{tot}, the plots are quite widely dispersed, while the plots are more closely aligned for high Re_{tot} values. This implies that close to the nozzle exit, varying the value of V_r has more of an impact at lower total mass flow rates, whereas the value of V_r is insignificant at higher Re_{tot} values.

In the region spanning from the local minimum in the Nu_x profile, *i.e.*, the estimated merge point, until the location of the local maximum, the greatest variance can be observed between V_r plots for all Re_{tot} values investigated. In general, the value of the Nu_x minimum is greater for higher V_r values, and thus the increase in Nu_x beyond this point is sharper for lower V_r values. This is consistent with the findings of Vishnuvardhanarao and Das [6], who noted that Nu_x is always greater when Re_w is larger than Re_o. For larger Re_{tot} values in this investigation, *i.e.*, $Re_{tot} = 18000$ (Fig. 7(c)) and $Re_{tot} = 20000$ (Fig. 7(d)), it can be inferred from their respective Nu_x plots that the greatest $\overline{Nu_x}$ value occurs when V_r is highest. This is not necessarily the case for lower Re_{tot}, such as $Re_{tot} = 14000$ (Fig. 7(a)) and $Re_{tot} = 16000$ (Fig. 7(b)), as the 'peaking' that takes place in the vicinity of the local maximum for smaller V_r drives up the value of $\overline{Nu_x}$, the prominence of which is greatest for the lowest Re_{tot} and V_r combination.

Finally, it is interesting to note the change in the location of the estimated merge point with V_r. For $Re_{tot} = 14000$, the location of the Nu_x minimum moves downstream with increasing V_r, suggesting that raising V_r delays the onset of the jet interaction. Conversely, a higher V_r seems to move the merge point upstream towards the nozzle exit for all higher Re_{tot} investigated in Fig. 7, except for $V_r = 0.5$ when $Re_{tot} = 16000$ and 20000, in which case the local Nu_x minimum moves upstream unexpectantly.

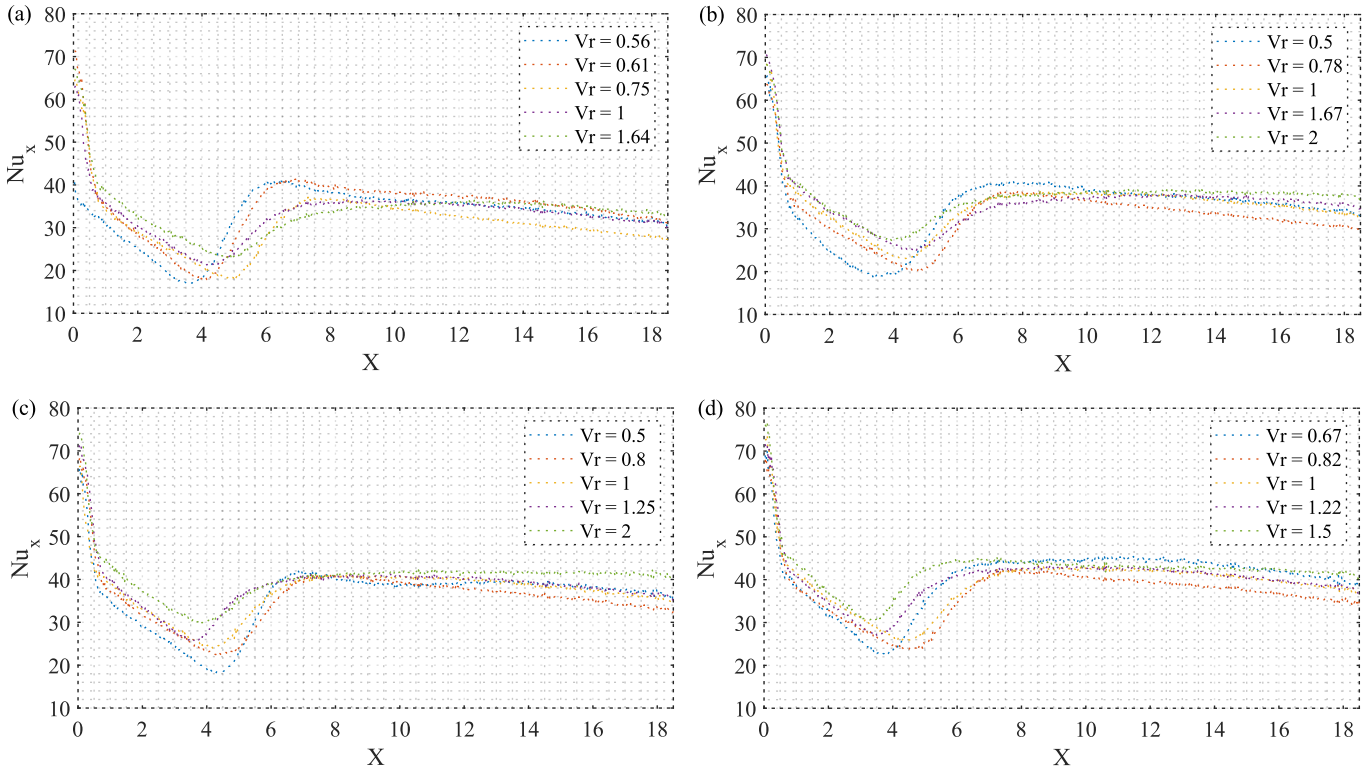

Fig. 7. Effect of changing velocity ratio V_r for a constant total Reynolds number Re_{tot}, where a) $Re_{tot} = 14000$, b) $Re_{tot} = 16000$, c) $Re_{tot} = 18000$ and d) $Re_{tot} = 20000$

IV. Conclusions

The present study experimentally investigates the effect of velocity ratio on the heat transfer characteristics of dual jet flow for a constant offset ratio of $OR = 3$. A uniform heat flux of 2500 W/m^2 is maintained in the bounding wall throughout testing and the surface temperature distribution is captured using an infra-red camera. The Reynolds number of each jet is varied separately from $5500 \leq Re \leq 12000$ to obtain a wide range of velocity ratio values. The heat transfer results are analyzed with respect to the time-averaged Nusselt number downstream profile Nu_x, where the effect of changing both the total mass flow rate and the velocity ratio V_r are investigated.

The results presented show that although the overall trend associated with the Nu_x profile remains relatively consistent throughout, the mass flow rate and the velocity ratio greatly impact the observed heat transfer behaviour. Compared to the single wall jet or single offset jet, the Nu_x profile associated with dual jet flow is distinctly different and possesses an additional level of control. While the heat transfer behavior associated with a single wall or offset jet for a given nozzle type can be altered only through adjusting the mass flow rate, the location of the relevant Nu_x maxima or minima generally remain consistent. Conversely, the ability to control the location of the local Nu_x minimum or maximum in the case of a dual jet through adjusting either the velocity ratio or the mass flow rate can prove advantageous for numerous applications, for example electronics cooling, where it may be necessary to tune the Nu_x maximum to coincide with a localized hot-spot.

The main findings of the study are as follows:

- For a constant velocity ratio, increasing the total mass flow rate enhances Nu_x at all downstream locations and moves the local Nu_x minimum towards the nozzle exit, indicating that the onset of the jet interactions occurs further upstream.
- The location of the local maximum remains consistent for a given V_r, however 'peaking' was found to occur in this region for a low V_r and R_{tot} combination.
- For a given mass flow rate, the effect of changing V_r on Nu_x is minimal in the far downstream region, where the jets approach self-similarity, however high V_r values appear to have a 'flattening' effect.
- Close to the nozzle exit, the effect of varying V_r is greatest for lower R_{tot} values, where the local Nu_x minimum moves downstream with increasing V_r. Conversely, the position of the local Nu_x minimum moves upstream with increasing V_r for all greater R_{tot} values examined.
- For higher total mass flow rates, $\overline{Nu_x}$ is greatest for larger V_r values. However, due to the peaking that can take place at the local maximum for lower Re_{tot} values, the maximum $\overline{Nu_x}$ can occur at smaller V_r values for lower total mass flow rates.

Further work is required however to examine the time-resolved effect of the velocity ratio, specifically to investigate the onset of instabilities of the dual jet flow and the effect this has on the overall heat transfer behaviour. In addition to this, the

effect of the offset ratio is yet to be analyzed through experimental means, and whether or not the trends observed in the current investigation remain consistent for varied OR values. Finally, the underlying fluid flow phenomenon driving the present Nu_x trends are not yet fully defined and hence an experimental flow imaging investigation is required ($e.g.$, via particle image velocimetry) to fully characterize dual jet flow in the context of this investigation.

REFERENCES

[1] S. K. Rathore and M. K. Das, "Comparison of two low-Reynolds number turbulence models for fluid flow study of wall bounded jets," (in English), *International Journal of Heat and Mass Transfer,* vol. 61, pp. 365-380, 2013, doi: 10.1016/j.ijheatmasstransfer.2013.01.062.

[2] T. Mondal, N. Srivastava, S. M. O'Shaughnessy and S. Pramanik, "Comparison of the mean flow and turbulence characteristics of a single offset jet and a dual offset jet," *European Journal of Mechanics - B/Fluids,* vol. 98, pp. 161-179, 2023, doi: 10.1016/j.euromechflu.2022.12.003.

[3] A. Kumar and M. K. Das, "Study of a Turbulent Dual Jet Consisting of a Wall Jet and an Offset Jet," *Journal of Fluids Engineering,* vol. 133, no. 10, 2011, doi: 10.1115/1.4004823.

[4] N. Gao, C. Y. Ching, D. Ewing and J. W. Naughton, "Flow and heat transfer measurements in a planar offset attaching jet with a co-flowing wall jet," *International Journal of Heat and Mass Transfer,* vol. 78, pp. 721-731, 2014, doi: 10.1016/j.ijheatmasstransfer.2014.07.008.

[5] X. K. Wang and S. K. Tan, "Experimental investigation of the interaction between a plane wall jet and a parallel offset jet " *Experiments in Fluids,* vol. 42, no. 4, pp. 551-562, 2007, doi: 10.1007/s00348-007-0263-9.

[6] E. Vishnuvardhanarao and M. K. Das, "Study of the heat transfer characteristics in turbulent combined wall and offset jet flows," *International Journal of Thermal Sciences,* vol. 48, no. 10, pp. 1949-1959, 2009, doi: 10.1016/j.ijthermalsci.2009.02.020.

[7] T. Mondal and S. M. O'Shaughnessy, "Numerical investigation of conjugate heat transfer to a turbulent dual offset jet," *International Journal of Thermal Sciences,* vol. 180, p. 107716, 2022, doi: 10.1016/j.ijthermalsci.2022.107716.

[8] Z. Li, W.-x. Huai and J. Han, "Large eddy simulation of the interaction between wall jet and offset jet," *Journal of Hydrodynamics, Ser. B,* vol. 23, no. 5, pp. 544-553, 2011, doi: 10.1016/S1001-6058(10)60148-5.

[9] T. Mondal, M. K. Das and A. Guha, "Numerical investigation of steady and periodically unsteady flow for various separation distances between a wall jet and an offset jet," *Journal of Fluids and Structures,* vol. 50, pp. 528-546, 2014, doi: 10.1016/j.jfluidstructs.2014.07.009.

[10] S. Farooq and M. Das, "Simulation of Thermal Characteristics of Turbulent Dual Jets," *J Appl Mech Eng,* vol. 3, no. 141, p. 2, 2014.

[11] A. Kumar, "Mean Flow and Thermal Characteristics of a Turbulent Dual Jet Consisting of a Plane Wall Jet and a Parallel Offset Jet," *Numerical Heat Transfer, Part A (Applications),* vol. 67, no. 10, pp. 1075-96, 2015, doi: 10.1080/10407782.2014.955348.

[12] T. Mondal, A. Guha and M. Kumar Das, "Analysis of Conjugate Heat Transfer for a Combined Turbulent Wall Jet and Offset Jet," *Journal of Heat Transfer,* vol. 138, no. 5, 2016, doi: 10.1115/1.4032287.

[13] N. Hnaien, S. Marzouk, H. B. Aissia and J. Jay, "Wall inclination effect in heat transfer characteristics of a combined wall and offset jet flow," *International Journal of Heat and Fluid Flow,* vol. 64, pp. 66-78, 2017, doi: 10.1016/j.ijheatfluidflow.2017.01.010.

[14] N. Hnaien, S. Marzouk, H. Ben Aissia and J. Jay, "CFD investigation on the offset ratio effect on thermal characteristics of a combined wall and offset jets flow," *Heat and Mass Transfer,* journal article vol. 53, no. 8, pp. 2531-2549, 2017, doi: 10.1007/s00231-017-2000-0.

[15] S. K. Rathore, A. Pathak, A. Majumdar and S. Chaudhuri, "Computational Investigation of Mixed Convection Heat Transfer from Laminar Offset Jet and Wall Jet," presented at the Fifth International Conference on Computational Methods for Thermal Problems, Bangalore, India, 2018.

[16] A. Assoudi, N. Mahjoub Saïd, H. Bournot and G. Le Palec, "Comparative study of flow characteristics of a single offset jet and a turbulent dual jet," *Heat and Mass Transfer,* vol. 55, no. 4, pp. 1109-1131, 2019, doi: 10.1007/s00231-018-2493-1.

[17] T. P. Singh, A. Kumar and A. K. Satapathy, "Heat Transfer and Fluid Flow Characteristics of a Turbulent Dual Jet Impinging on a Wavy Surface," *Journal of Thermal Science and Engineering Applications,* vol. 12, no. 4, 2020, doi: 10.1115/1.4045882.

[18] N. Hnaien, T. Mondal, M. Ajmi, S. Marzouk, W. Aich and L. Kolsi, "Numerical study on mean flow characteristics for a combined turbulent wall and offset jets with a parallel co-flow," *Journal of Taibah University for Science,* vol. 16, no. 1, pp. 732-748, 2022, doi: 10.1080/16583655.2022.2109936.

[19] T. Mondal, N. Hnaien, M. Ajmi, K. Ghachem and L. Kolsi, "CFD Investigation of Thermal Characteristics for a Dual Jet with a Parallel Co-flow," *ACS Omega,* vol. 7, no. 32, pp. 27864-27875, 2022, doi: 10.1021/acsomega.2c00609.

[20] P. Murphy, S. Alimohammadi and S. O. Shaughnessy, "Experimental Analysis of Heat Transfer to a Dual Jet Flow: Effect of Reynolds Number," in *2022 28th International Workshop on Thermal Investigations of ICs and Systems (THERMINIC)*, 28-30 Sept. 2022 2022, pp. 1-6, doi: 10.1109/THERMINIC57263.2022.9950682.

[21] A. Nasr and J. C. S. Lai, "A turbulent plane offset jet with small offset ratio," *Experiments in Fluids,* vol. 24, no. 1, pp. 47-57, 1998, doi: 10.1007/s003480050149.

[22] R. D. Mehta and P. Bradshaw, "Design rules for small low speed wind tunnels," *The Aeronautical Journal,* vol. 83, no. 827, pp. 443-453, 1979, doi: 10.1017/S0001924000031985.

[23] T. Morel, "Design of Two-Dimensional Wind Tunnel Contractions," *Journal of Fluids Engineering,* vol. 99, no. 2, pp. 371-377, 1977, doi: 10.1115/1.3448764.

[24] M. J. Gibbons, A. I. Garivalis, S. O'Shaughnessy, P. Di Marco and A. J. Robinson, "Evaporating hydrophilic and superhydrophobic droplets in electric fields," *International Journal of Heat and Mass Transfer,* vol. 164, p. 120539, 2021, doi: 10.1016/j.ijheatmasstransfer.2020.120539.

[25] R. S. AbdulNour, K. Willenborg, J. J. McGrath, J. F. Foss and B. S. AbdulNour, "Measurements of the convection heat transfer coefficient for a planar wall jet: uniform temperature and uniform heat flux boundary conditions," *Experimental Thermal and Fluid Science,* vol. 22, no. 3, pp. 123-131, 2000, doi: 10.1016/S0894-1777(00)00018-2.

[26] D. S. Kim, S. H. Yoon, D. H. Lee and K. C. Kim, "Flow and heat transfer measurements of a wall attaching offset jet," *International Journal of Heat and Mass Transfer,* vol. 39, no. 14, pp. 2907-2913, 1996, doi: 10.1016/0017-9310(95)00383-5.